Electronic Supplementary Information

5,6-Fused Bicyclic Tetrazolo-Pyridazine Energetic Materials

Sitong Chen[a], Yuji Liu[a], Yongan Feng[a], Xianjin Yang[b] and Qinghua Zhang*[a]

[a] Institute of Chemical Materials, China Academy of Engineering Physics (CAEP), Mianyang, 621900, P. R. China. E-mail: qinghuazhang@caep.cn.
[b] School of Chemistry and Molecular Engineering, East China University of Science and Technology, Shanghai, P. R. China.

Table of Contents

1. General information

Caution!!: Although we have not experienced any difficulties in preparing and handling these new compounds. These compounds are energetic materials and tend to explode under certain conditions. Thus, proper protective precautions must be used. Safety equipment such as anti-cutting gloves, leather coats, face shields, and ear plugs are recommended. And all compounds should be handled with very care.

General methods: All reagents were obtained commercially and were used as received. ^{1}H and ^{13}C NMR spectra were recorded on a Bruker 600 AVANCE spectrometer (600 and 151 MHz, respectively) with an internal standard (^{1}H NMR: DMSO at 2.50 ppm, CD_3CN at 1.94 ppm; ^{13}C NMR: DMSO at 39.52 ppm, CD_3CN at 118.26 ppm). Infrared (IR) spectra were recorded on an Perkin-Elmer Spectrum II IR Spectrometers using KBr pellets. Densities were determined by a Micromeritics Accupyc II 1340 gas pycnometer at room temperature. Elemental analyses (C, H, N) were performed on a Vario Micro cube elemental analyzer. Thermal decomposition temperatures were determined by using differential thermal analysis (DTA) on an OZM DTA 552-Ex differential thermal analyzer, differential scanning calorimetry (DSC) and thermogravimetric analysis (TGA) on a Mettler-Toledo TGA/DSC 1 Star^e system at a heating rate of 10 °C·min^{-1} from 50 °C to 450 °C under dry oxygen-free nitrogen atmosphere. The heats of formation were calculated based on the method developed by Byrd and Rice in 2006. The detonation parameters, including detonation velocity (*vD*) and detonation pressure (*P*), were calculated by using the EXPLO5 (version 6.02) code. The impact and friction sensitivities were measured on a standard BAM fall hammer and a BAM friction tester. Hirshfeld surfaces and 2D fingerprint plots were generated by CrystalExplorer (version 17.5)[S1]. Iso-chemical shielding surfaces (ICSS) and localized orbital locator-π (LOL-pi) maps were analyzed and drawn by using Multiwfn (version 3.5)[S2] and Visual Molecular Dynamics (VMD, version 1.9.3) program suites[S3]. The bond dissociation enthalpies (*BDEs*) were calculated using B3LYP/6-311++g** level.

2. Synthesis

Synthesis of 4-amino-3,6-dichloro-5-nitropyridazine (p2) and 3,5-diamino- 6-chloro-4-nitro-pyridazine (p3): To a mixture of 10ml conc. H_2SO_4 and 4ml fuming HNO_3 at 0°C, 4g 4-amino-3,6-dichloropyridazine (**p1**) was slowly added in small batches with continuous stirring. The temperature was allowed to warm slowly to room temperature and held for 4 hours. Then the solution was poured into ice (about 35g) with stirring. The formed solid was filtered and washed with small amount of water to obtain 4.64g (91% yield) of 4-amino-3,6-dichloro-5-nitro- pyridazine (**p2**). Single crystal suitable for single-crystal X-ray diffraction could be obtained through recrystallization from dichloromethane. The solid was used to synthesize **p3** immediately so as to avoid the hydrolytic action, which turns the 6-chloro into carbanyl group. The above 4.64g solid was added into a mixture of 20ml 25% aqua ammonia and 80ml anhydrous ethanol. This mixture was sealed in a Synthware thick-walled pressure bottle and heated to 96°C with stirring for one hour. After cooling to room temperature, the resulting orange crystalline solid was filtered and washed with water and anhydrous ethanol. It was dried to give 3,5-diamino- 6-chloro-4-nitro-pyridazine (**p3**), yielded 3.31g (95%). ^{1}H NMR (DMSO-d_6): 8.27 (b, 2H), 7.73 (s, 2H); ^{13}C NMR (DMSO-d_6): 153.21, 149.64, 135.41, 115.98, ppm. HRMS (ESI-) (m/z) calcd for $C_4H_3N_5O_2Cl^-$ 187.9981, found 188.0024. IR (KBr pellet): 3784, 3498, 3422, 3377, 3252, 2935, 2869, 2314, 2123, 1609, 1497, 1456, 1402, 1317, 1289, 1185, 1113, 1032, 884, 776, 731, 703, 615, 557, 475, cm^{-1}. Elemental analysis (%) for $C_4H_4N_5O_2Cl$ (189.56): calcd: C, 25.35; H, 2.13; N, 36.95; found: C 25.29, H 2.07, N 36.88.

Synthesis of 6,8-diamino-7-nitrotetrazolo[1,5-b]pyridazine (1): To a suspension of 2.87g 3,5-diamino-6-chloro-4-nitro-pyridazine (**p3**) in 30ml N,N-dimethylformamide (DMF), 1.06g sodium azide (NaN_3) was added with stirring in small portions at 0°C. The mixture was then heated to 96°C and reacted for 10 hours. The solution was diluted with a large amount of water until no more precipitates were obtained. The precipitates were filtered, washed with water and ethanol, and dried in air to get 6,8-diamino-7-nitrotetrazolo[1,5-b]pyridazine semihydrate (**1**$\cdot 0.5H_2O$, yellow). Yield 2.70g (87%). Crystal suitable for X-ray single-crystal diffraction could be obtained through recrystallization in methanol ($1\cdot 0.5H_2O$). The anhydrous sample could be prepared by heating the semihydrous sample at 140°C for 5 hours. All the tests were completed using the anhydrous sample. ^{1}H NMR (DMSO-d_6): 10.03 (s, 1H), 9.59 (s, 1H), 7.76 (s, 2H); ^{13}C NMR (DMSO-d_6): 152.78, 141.84, 137.92, 113.69, ppm. HRMS (ESI-) (m/z) calcd for $C_4H_3N_8O_2^-$ 195.0384, found 195.0419. IR (KBr pellet): 3553, 3441, 3360, 3300, 3238, 2174, 1651, 1619, 1583, 1511, 1470, 1427, 1339, 1279, 1136, 1092, 1070, 895, 840, 739, 681, 630, 587, 517, cm^{-1}. Elemental analysis (%) for $C_4H_4N_8O_2$ (196.13): calcd: C, 24.50; H, 2.06; N, 57.13; found: C 24.42, H 2.00, N 57.05.

Synthesis of 8-amino-6,7-dinitrotetrazolo[1,5-b]pyridazine (2): A mixture of 50 mL of acetonitrile and 1 mL of water was cooled to -12°C with an ice salt bath (in a Dewar flask). A fluorine:nitrogen gas mixture (20:80) was bubbled through the acetontrile solution for 2.5 h at -12°C. The gases were quantified by transferring the gases through a 15L bottle, of which the initial pressure was 0.14 MPa. Compound **1** (0.75 g, 4.88 mmol) was added portionwise at this temperature. The reaction was stirred at -8°C for 1 h and then allowed to be warmed to room temperature with continuous stirring for 15 h. The formed clear solution was concentrated. The product was purified by flash chromatography with 1:5 EtOAc:PE as eluent. A crystalline cyan solid was obtained from the slow volatilization of the solution, yielding 0.20 g (18.1%). ^{1}H NMR (CD_3CN): 9.26 (s, 1H), 9.10 (s, 1H); ^{13}C NMR (CD_3CN): 154.33, 143.42, 142.19, 115.38, ppm. HRMS (ESI-) (m/z) calcd for $C_4HN_8O_4^-$ 225.0126, found 225.0145. IR (KBr pellet): 3453, 3397, 3332, 3213, 2932, 1655, 1634, 1572, 1494, 1409, 1370, 1327, 1306, 1278, 1156, 1107, 1066, 1020, 983, 889, 839, 778, 752, 727, 697, 638, 609, 574, cm^{-1}. Elemental analysis (%) for $C_4H_2N_8O_4$ (226.11): calcd: C, 21.25; H, 0.89; N, 49.56; found: C 21.14, H 0.79, N 49.47.

3. ^{1}H and ^{13}C NMR spectra

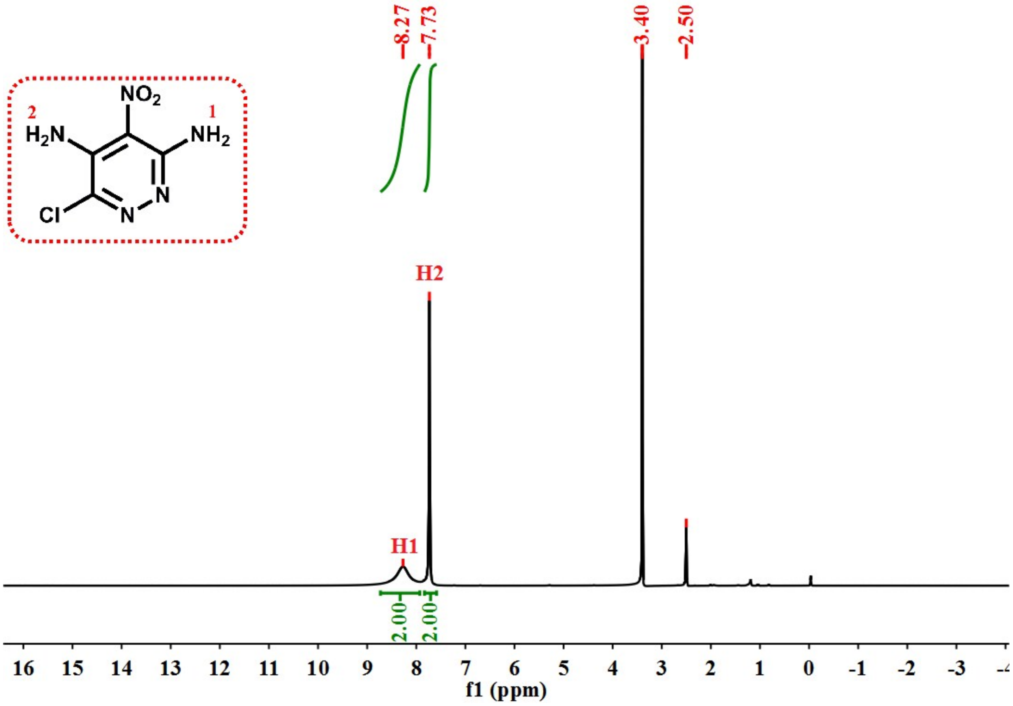

Fig. S1 ^{1}H NMR of **p3** (DMSO-d_6)

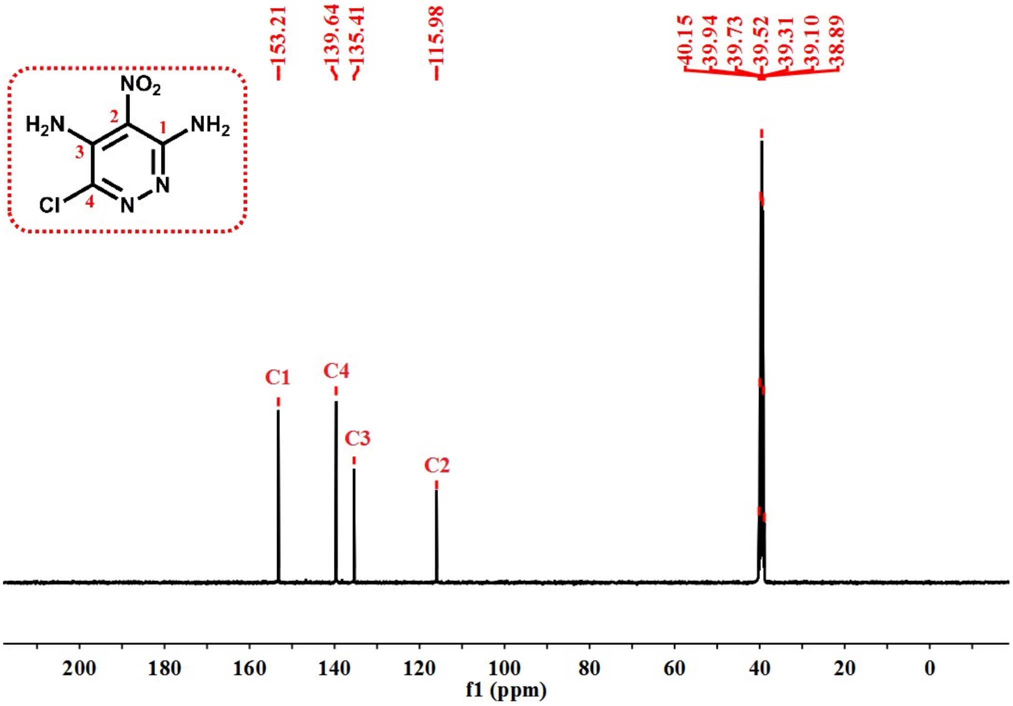

Fig. S2 ^{13}C NMR of **p3** (DMSO-d_6)

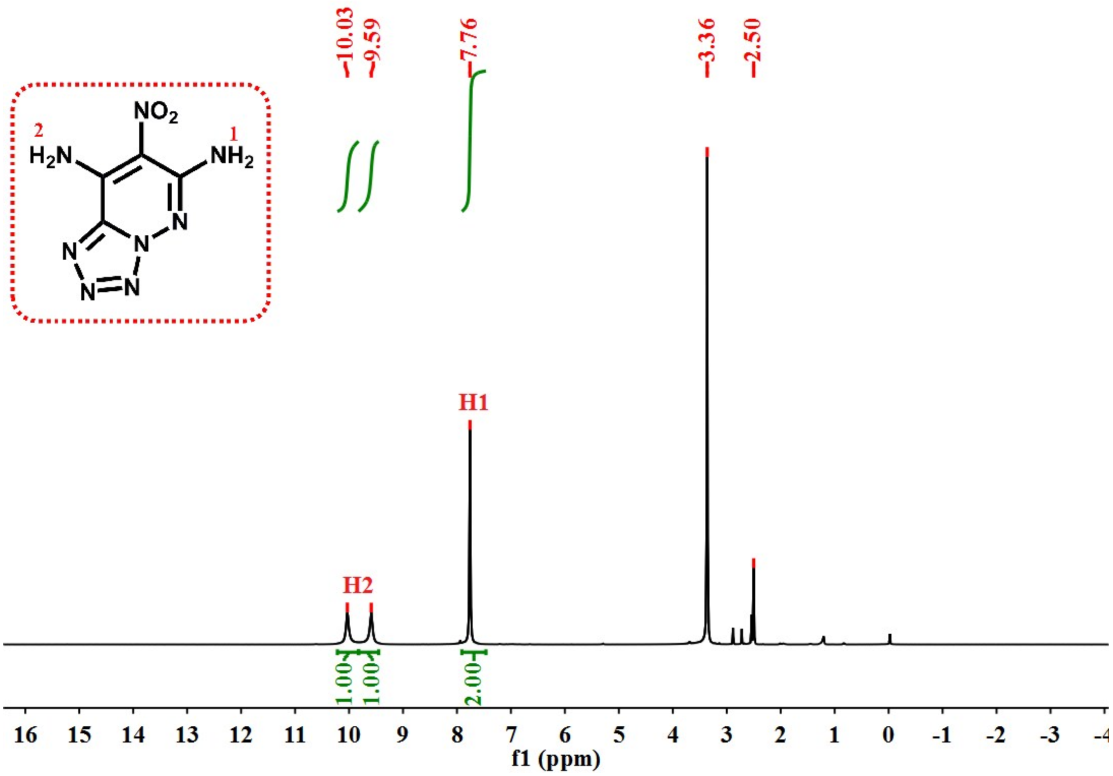

Fig. S3 ^{1}H NMR of **1** (DMSO-d_6)

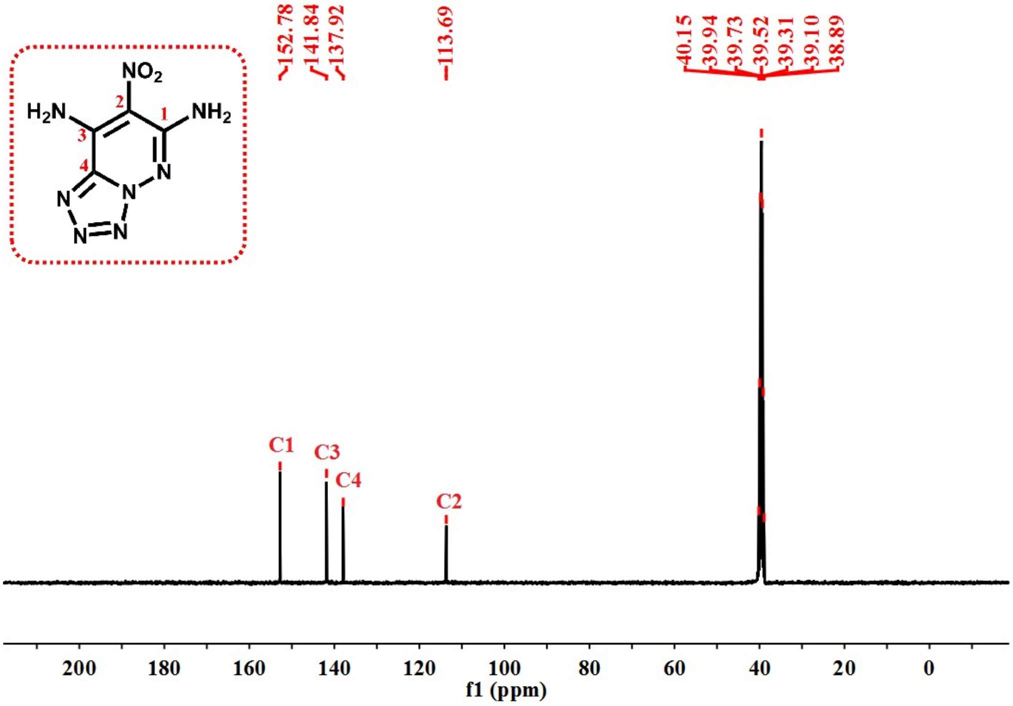

Fig. S4 ^{13}C NMR of **1** (DMSO-d_6)

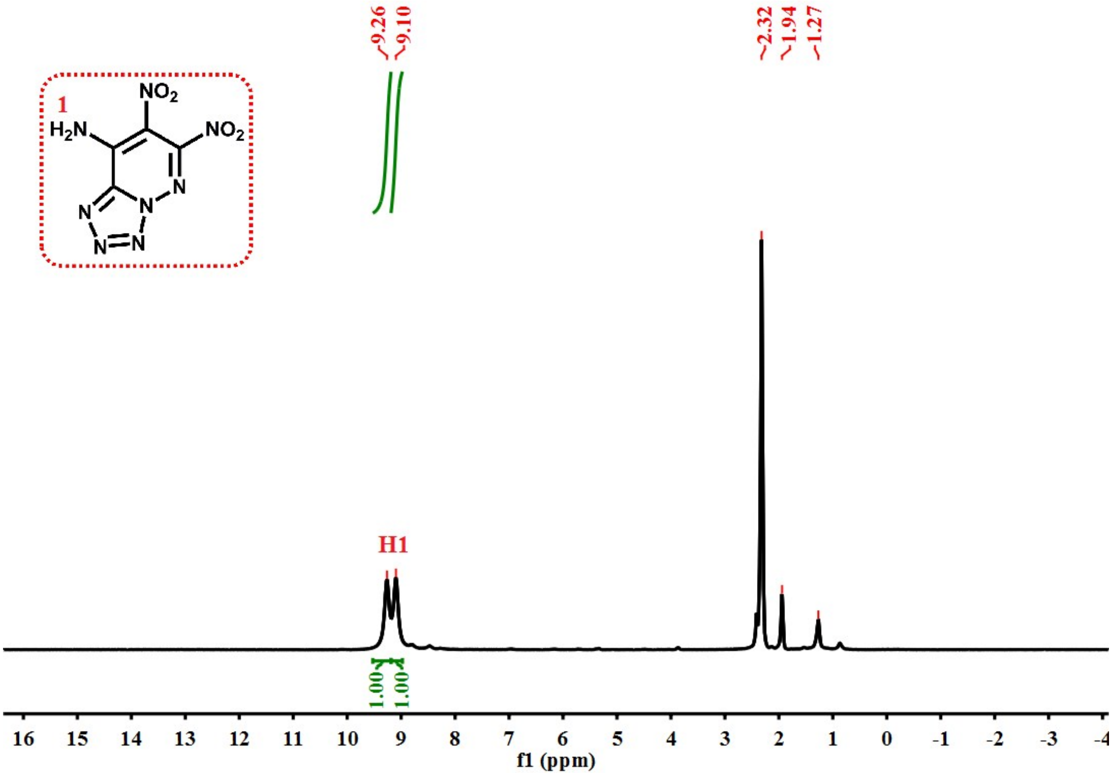

Fig. S5 ^{1}H NMR of **2** (CD_3CN)

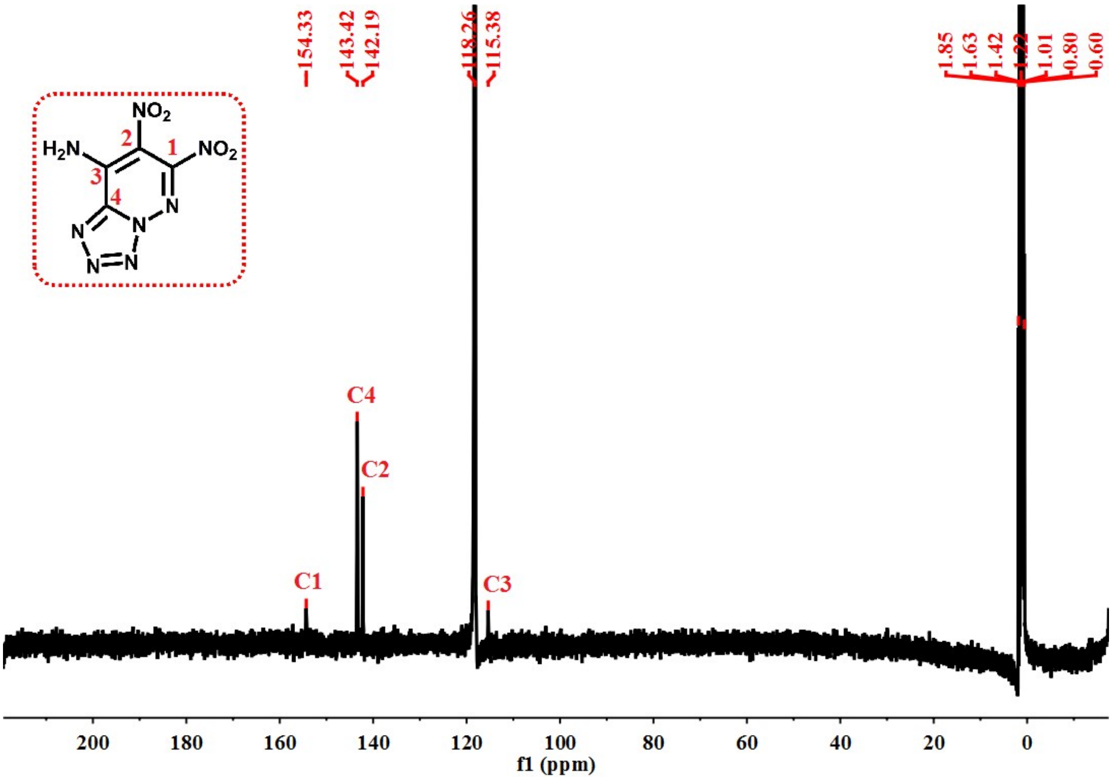

Fig. S6 ^{13}C NMR of **2** (CD_3CN)

4. Mass spectra

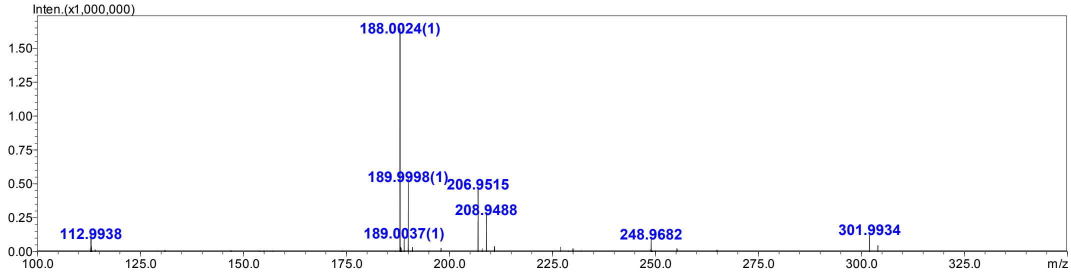

Fig. S7 mass spectra of **p3** (calcd for $C_4H_3N_5O_2Cl^-$ 187.9981)

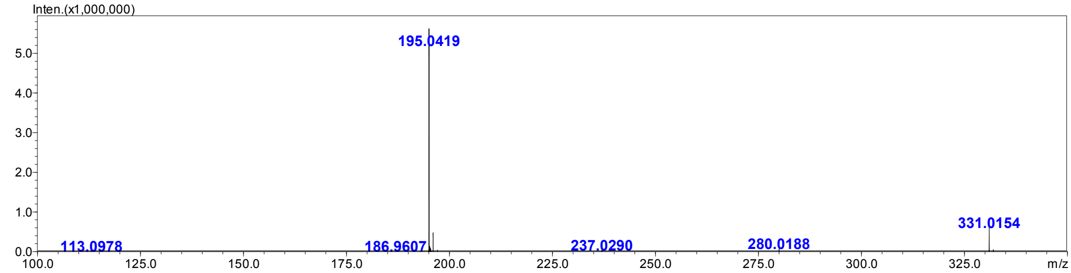

Fig. S8 mass spectra of **1** (calcd for $C_4H_3N_8O_2^-$ 195.0384)

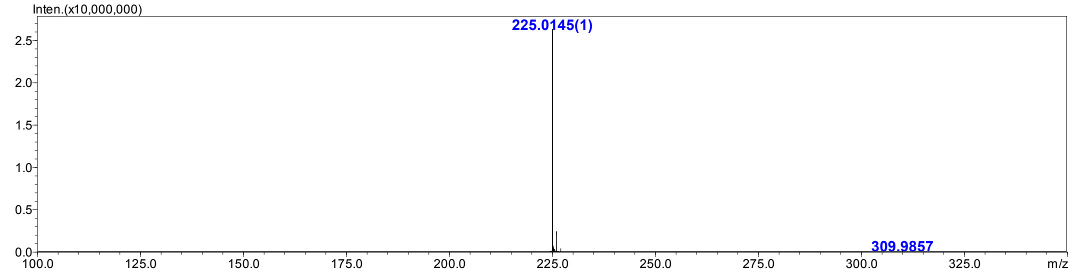

Fig. S9 mass spectra of **2** (calcd for $C_4HN_8O_4^-$ 225.0126)

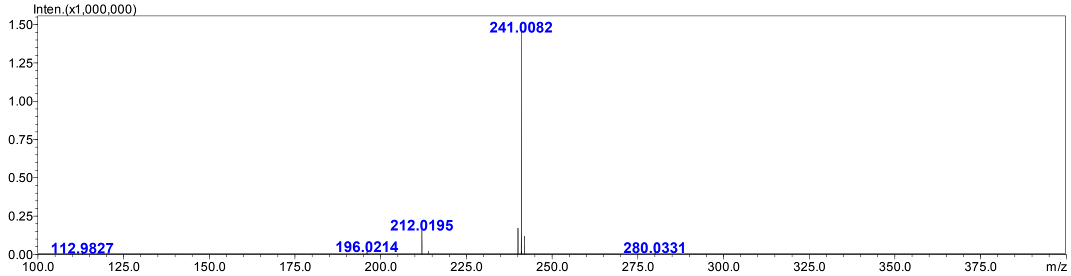

Fig. S10 mass spectra of **3** (calcd for $C_4HN_8O_5^-$ 241.0075)

5. IR Curves

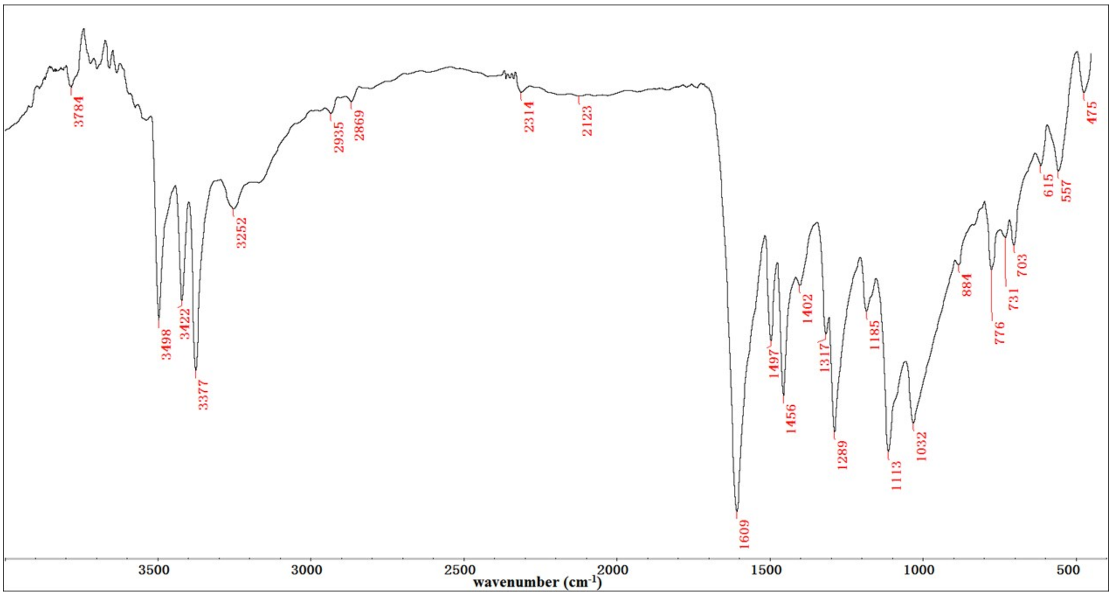

Fig. S11 IR curve of **p3**

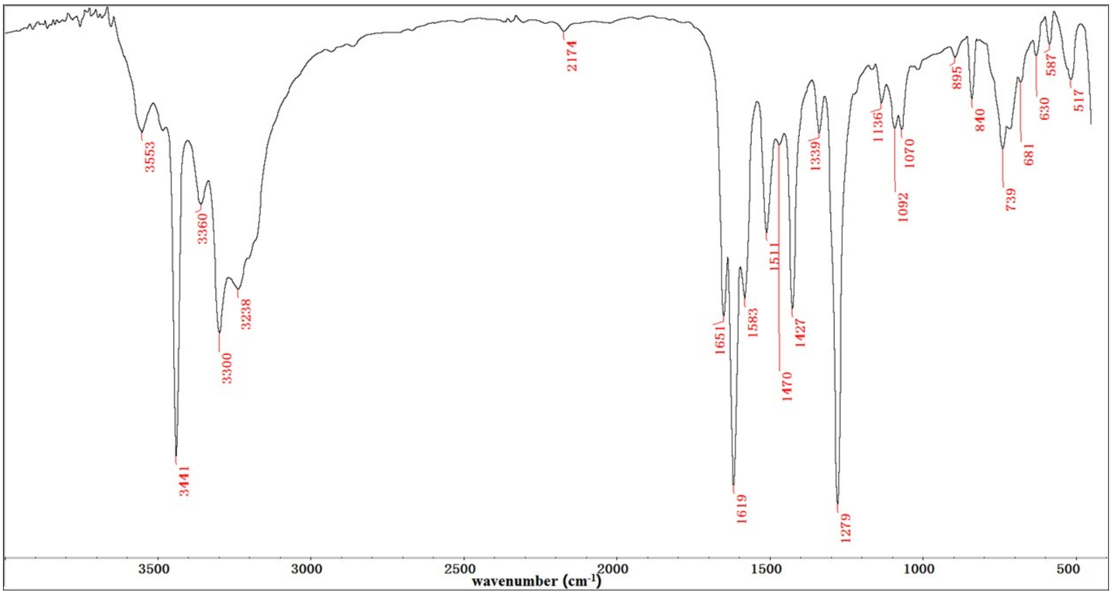

Fig. S12 IR curve of **1**

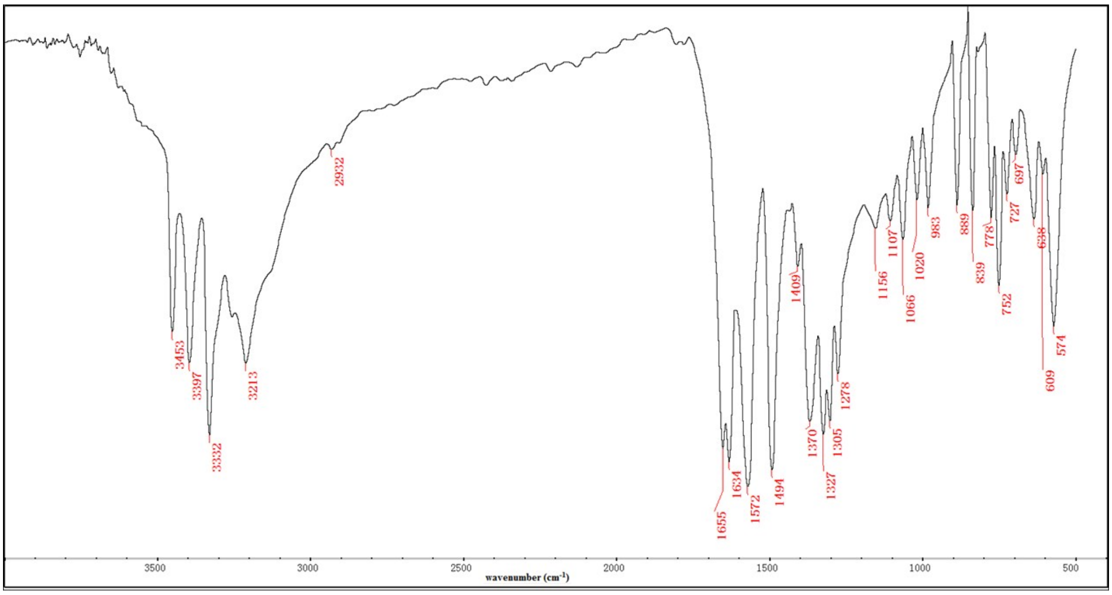

Fig. S13 IR curve of **2**

6. X-ray Crystallography

The crystal structure was determined by single-crystal X-ray diffraction with a Rigaku AFC-10/Saturn 724⁺CCD diffractometer with graphite-monochromated Mo Kα radiation (λ=0.71073 Å) using the multi-scan technique. Data collection and reduction were performed with CrysAlisPro. The structure was solved with SHELXS, refined with SHELXL-97, and checked with PLATON, all integrated into the Olex2/1.2 software suite[S4]. The finalized CIF file was checked with checkCIF. Interlamellar spacing were analyzed with Mercury/3.10.2[S5]. Illustrations of crystal structures were drawn with Diamond/3.2[S6].

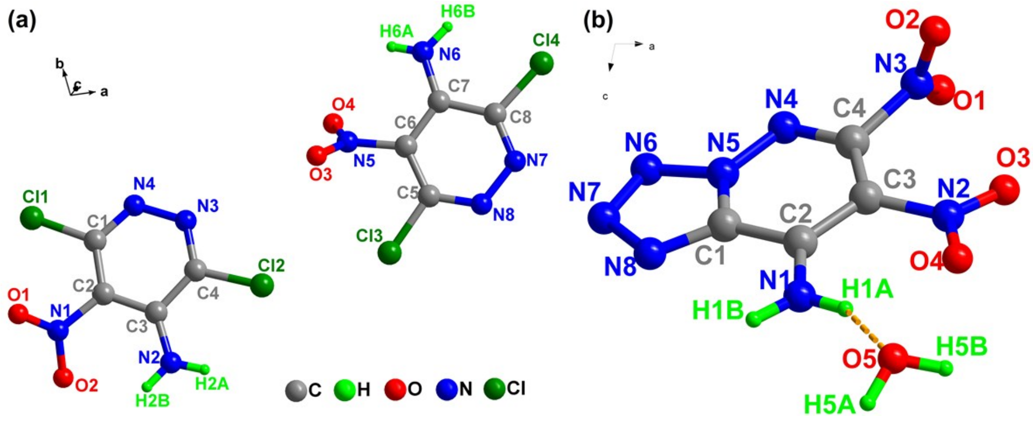

Fig. S14 (a) Crystal structure of **p2**; (b) Crystal structure of **2**·H_2O

Table S1. Crystal data and details of the structure determination

	p2	**1**·$0.5H_2O$	**2**	**2**·H_2O
CCDC No.	1947089	1947090	1952870	1952871
Empirical Formula	$C_4H_2Cl_2N_4O_2$	$C_8H_{10}N_{16}O_5$	$C_4H_2N_8O_4$	$C_4H_4N_8O_5$
Formula	209.00	410.32	226.14	244.15

Weight				
Temperature (K)	227.0	100.0	100.0	100.0
Wavelength (Å)	0.71073	0.71073	0.71073	0.71073
Crystal System	monoclinic	monoclinic	monoclinic	monoclinic
Space group	$P2_1/c$	C2/c	$P2_1/c$	C2/c
a (Å)	16.0864(10)	12.2036(15)	11.6487(5)	23.411(3)
b (Å)	12.7175(8)	4.6757(5)	9.8870(5)	5.0229(5)
c (Å)	7.1186(5)	25.698(3)	14.4221(7)	15.2453(19)
β (°)	99.450(2)	93.484(7)	106.486(2)	101.545(4)
Volume (Å^3)	1436.55(16)	1463.6(3)	1636.5(4)	1756.5(4)
Z	8	4	8	8
Density (g·cm^{-3})	1.933	1.862	1.886	1.847
μ (mm^{-1})	0.861	0.157	0.168	0.168
F(000)	832.0	840.0	912.0	992.0
Crystal Size (mm^3)	0.10 × 0.12 × 0.20	0.12 × 0.08 × 0.06	0.11 × 0.08 × 0.06	0.11 × 0.05 × 0.04
Index ranges	$-20 \leq h \leq 20$ $-16 \leq k \leq 16$ $-8 \leq l \leq 9$	$-13 \leq h \leq 15$ $-6 \leq k \leq 5$ $-33 \leq l \leq 33$	$-15 \leq h \leq 15$ $-10 \leq k \leq 12$ $-18 \leq l \leq 16$	$-28 \leq h \leq 27$ $-6 \leq k \leq 5$ $-19 \leq l \leq 14$
2θ range for data collection (°)	5.14 to 55.16	6.68 to 55.02	5.06 to 55.00	5.46 to 52.82
Reflections collected	16870	5433	12802	5703
Independent reflections	3286 [R_{int} = 0.0646, R_{sigma} = 0.0463]	1659 [R_{int} = 0.0937, R_{sigma} = 0.0913]	3606 [R_{int} = 0.0969, R_{sigma} = 0.1061]	1771 [R_{int} = 0.0673, R_{sigma} = 0.0789]
Data/restraints/parameters	3286/0/233	1659/0/153	3606/0/289	1771/0/157
Goodness-of-fit on F^2	1.062	1.023	1.052	1.066
Final R indexes [I>=2σ (I)]	R_1 = 0.0418 wR_2 = 0.0925	R_1 = 0.0511 wR_2 = 0.1038	R_1 = 0.0597 wR_2 = 0.1083	R_1 = 0.0567 wR_2 = 0.1167
Final R indexes [all data]	R_1 = 0.0561 wR_2 = 0.1002	R_1 = 0.1085, wR_2 = 0.1287	R_1 = 0.1329 wR_2 = 0.1415	R_1 = 0.1040, wR_2 = 0.1446
Largest diff. peak/hole (e·Å^{-3})	0.34/-0.35	0.35/-0.32	0.39/-0.41	0.39/-0.34

Table S2. Bond lengths of **1**·$0.5H_2O$.

Bond	Lengths (Å)	Bond	Lengths (Å)
O1-N2	1.242(3)	N7-N8	1.358(3)
O2-N2	1.242(3)	N7-C4	1.337(3)
O3-H3_a	0.88(3)	N8-C1	1.332(3)
O3-H3	0.88(3)	N1-H1A	0.86(3)
N1-C1	**1.333(3)**	N1-H1B	0.96(4)
N2-C2	**1.423(3)**	N3-H3A	0.92(4)
N3-C3	**1.324(3)**	N3-H3B	0.89(3)
N4-N5	1.348(3)	C1-C2	1.460(3)
N4-C4	1.334(3)	C2-C3	1.406(3)
N5-N6	1.319(3)	C3-C4	1.437(4)
N6-N7	1.348(3)		

Table S3. Bond angles of **1**·$0.5H_2O$

Bond angle	Angle (°)	Bond angle	Angle (°)
H3-O3-H3_a	108(3)	C3-N3-H3A	118(2)
O1-N2-C2	120.07(19)	H3A-N3-H3B	124(3)
O2-N2-C2	118.7(2)	N8-C1-C2	123.2(2)
O1-N2-O2	121.2(2)	N1-C1-N8	114.1(2)
N5-N4-C4	105.0(2)	N1-C1-C2	122.7(2)
N4-N5-N6	112.4(2)	N2-C2-C3	118.3(2)
N5-N6-N7	104.4(2)	N2-C2-C1	121.0(2)
N6-N7-C4	109.7(2)	C1-C2-C3	120.7(2)
N8-N7-C4	129.2(2)	N3-C3-C2	129.0(2)
N6-N7-N8	121.1(2)	N3-C3-C4	116.9(2)
N7-N8-C1	113.42(19)	C2-C3-C4	114.1(2)
C1-N1-H1A	113.8(19)	N4-C4-N7	108.5(2)
H1A-N1-H1B	124(3)	N4-C4-C3	132.0(2)
C1-N1-H1B	123(2)	N7-C4-C3	119.5(2)
C3-N3-H3B	118.2(17)		

Table S4. Hydrogen Bonds of **1**·$0.5H_2O$

H-Bond	Lengths D-H (Å)	Lengths H···A (Å)	Lengths D···A (Å)	Angle (°)
N1-H1A···N8	0.86(3)	2.25(3)	3.107(3)	176(2)
N1-H1B···O1	**0.96(4)**	**1.94(3)**	**2.603(3)**	**124(3)**
N1-H1B···O1	0.96(4)	2.32(3)	3.233(3)	158(3)
O3-H3.. N5	0.88(3)	2.26(3)	3.134(3)	178(3)
N3-H3A···O2	**0.92(4)**	**1.93(3)**	**2.577(3)**	**126(3)**
N3-H3A···O3	0.92(4)	2.24(3)	2.950(3)	134(3)
N3-H3A···N2	0.92(4)	2.62(3)	2.923(3)	100(2)
N3-H3B···N4	0.89(3)	2.59(3)	2.936(3)	104(2)

N3-H3B···N4	0.89(3)	2.11(3)	2.927(3)	152(2)
N3-H3B···N5	0.89(3)	2.62(3)	3.368(3)	142(2)

Table S5. Torsion angles of **1**·$0.5H_2O$

	Torsion angle (°)		Torsion angle (°)
O1-N2-C2-C1	**-5.3(3)**	N8-N7-C4-C3	1.2(4)
O1-N2-C2-C3	**175.4(2)**	N7-N8-C1-N1	179.9(2)
O2-N2-C2-C1	**174.4(2)**	N7-N8-C1-C2	0.3(3)
O2-N2-C2-C3	**-4.9(3)**	N1-C1-C2-N2	0.9(4)
C4-N4-N5-N6	-0.7(3)	N1-C1-C2-C3	-179.8(2)
N5-N4-C4-N7	0.9(3)	N8-C1-C2-N2	-179.5(2)
N5-N4-C4-C3	-179.2(3)	N8-C1-C2-C3	-0.1(4)
N4-N5-N6-N7	0.2(3)	N2-C2-C3-N3	-1.0(4)
N5-N6-N7-N8	178.6(2)	N2-C2-C3-C4	179.8(2)
N5-N6-N7-C4	0.4(3)	C1-C2-C3-N3	179.6(2)
N6-N7-N8-C1	-178.6(2)	C1-C2-C3-C4	0.4(3)
C4-N7-N8-C1	-0.9(4)	N3-C3-C4-N4	-0.1(4)
N6-N7-C4-N4	-0.9(3)	N3-C3-C4-N7	179.8(2)
N6-N7-C4-C3	179.2(2)	C2-C3-C4-N4	179.2(3)
N8-N7-C4-N4	-178.8(2)	C2-C3-C4-N7	-0.9(3)

Table S6. Bond lengths of **2**

Bond	Lengths (Å)	Bond	Lengths (Å)
O1-N2	1.229(3)	N8-C1	1.318(4)
O2-N2	1.227(4)	**N9-C6**	**1.317(4)**
O3-N3	1.214(4)	**N10-C7**	**1.439(4)**
O4-N3	1.202(4)	**N11-C8**	**1.489(4)**
O5-N10	1.227(4)	N12-N13	1.357(3)
O6-N10	1.224(4)	N12-C8	1.294(4)
O7-N11	1.224(3)	N13-N14	1.346(4)
O8-N11	1.215(4)	N13-C5	1.349(4)
N1-C2	**1.302(4)**	N14-N15	1.312(4)
N2-C3	**1.424(4)**	N15-N16	1.362(4)
N3-C4	**1.494(4)**	N16-C5	1.322(4)
N4-C4	1.296(4)	C1-C2	1.447(4)
N4-N5	1.362(4)	C2-C3	1.416(4)
N5-C1	1.341(4)	C3-C4	1.414(4)
N5-N6	1.349(4)	C5-C6	1.436(5)
N6-N7	1.312(3)	C6-C7	1.404(4)
N7-N8	1.360(4)	C7-C8	1.414(4)

Table S7. Bond angles of **2**

Bond angle	Angle (°)	Bond angle	Angle (°)
O1-N2-O2	122.8(3)	N15-N16-C5	105.1(2)
O1-N2-C3	118.6(3)	C6-N9-H9B	120
O2-N2-C3	118.7(3)	H9A-N9-H9B	120
O3-N3-O4	126.5(3)	C6-N9-H9A	120
O3-N3-C4	115.4(3)	N5-C1-N8	108.2(3)
O4-N3-C4	117.9(3)	N5-C1-C2	119.7(3)
N5-N4-C4	110.2(2)	N8-C1-C2	132.1(3)
N4-N5-N6	121.1(2)	N1-C2-C1	118.6(3)
N4-N5-C1	129.1(3)	N1-C2-C3	128.6(3)
N6-N5-C1	109.7(2)	C1-C2-C3	112.8(2)
N5-N6-N7	104.8(2)	N2-C3-C4	120.8(3)
N6-N7-N8	111.5(3)	C2-C3-C4	118.9(3)
N7-N8-C1	105.8(2)	N2-C3-C2	120.3(3)
H1A-N1-H1B	120	N4-C4-C3	129.0(3)
C2-N1-H1A	120	N3-C4-N4	109.1(2)
C2-N1-H1B	120	N3-C4-C3	121.9(3)
O5-N10-C7	118.4(2)	N13-C5-C6	119.6(3)
O5-N10-O6	124.4(3)	N13-C5-N16	108.7(3)
O6-N10-C7	117.2(3)	N16-C5-C6	131.6(3)
O7-N11-O8	125.9(3)	N9-C6-C5	118.6(3)
O7-N11-C8	116.3(3)	N9-C6-C7	128.2(3)
O8-N11-C8	117.7(2)	C5-C6-C7	113.2(3)
N13-N12-C8	110.5(3)	C6-C7-C8	118.9(3)
N12-N13-C5	128.6(3)	N10-C7-C6	120.9(3)
N12-N13-N14	122.1(3)	N10-C7-C8	119.9(3)
N14-N13-C5	109.4(3)	N11-C8-N12	109.5(2)
N13-N14-N15	104.9(3)	N11-C8-C7	121.7(3)
N14-N15-N16	112.0(2)	N12-C8-C7	128.8(3)

Table S8. Hydrogen Bonds of **2**

H-Bond	Lengths D-H (Å)	Lengths H···A (Å)	Lengths D···A (Å)	Angle (°)
N1-H1A···O1	**0.88**	**2.05**	2.638(4)	124
N1-H1A···N8	0.88	2.19	2.944(4)	143
N1-H1B···O1	0.88	2.4	**3.273(3)**	**175**
N1-H1B···O6	0.88	2.51	2.884(4)	107
N9-H9A···O2	0.88	2.3	3.129(4)	157
N9-H9A···O5	**0.88**	**2.07**	**2.666(3)**	**124**
N9-H9B···O7	0.88	2.38	3.012(3)	129

7. DTA\DSC and TG-DTG curves

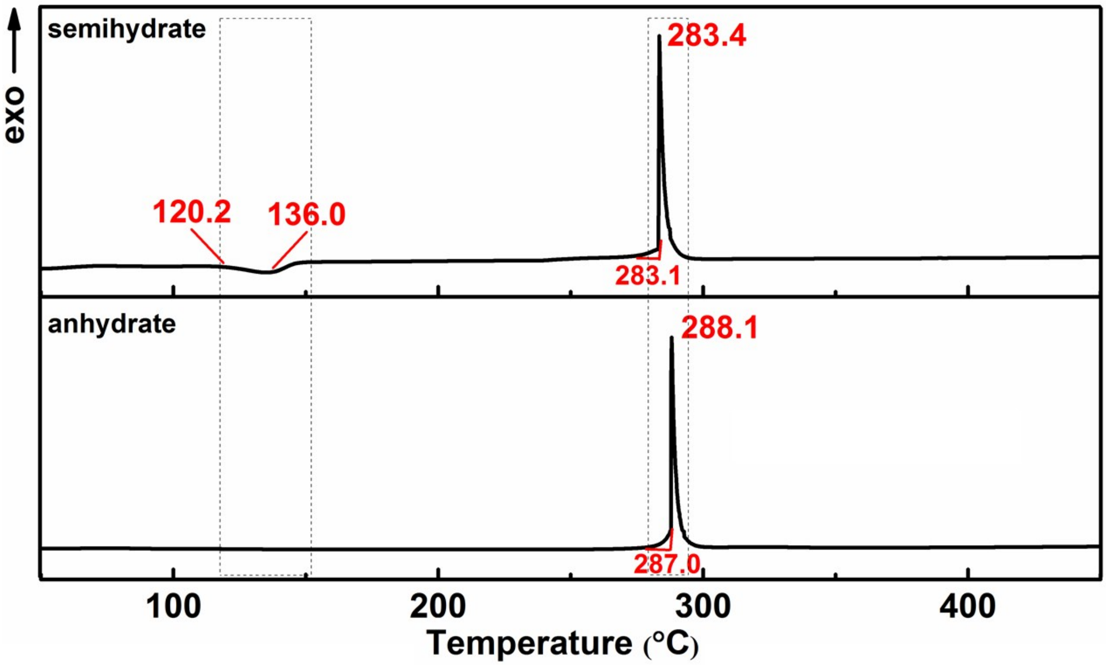

Fig. S15 DTA curves (10 °C·min^{-1}) of **1** and its semihydrate

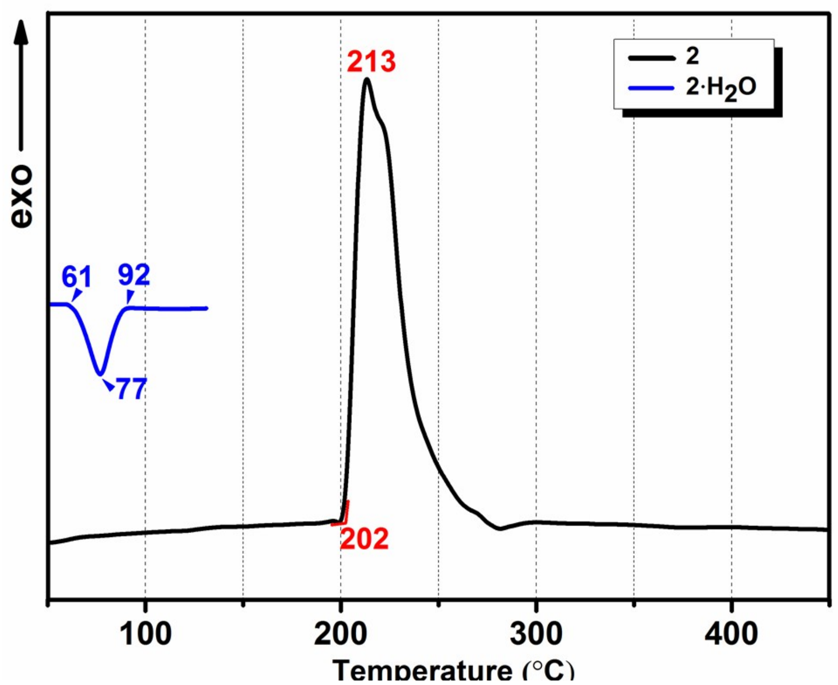

Fig. S16 DSC curves (10 °C·min^{-1}) of **2** and **2**·H_2O

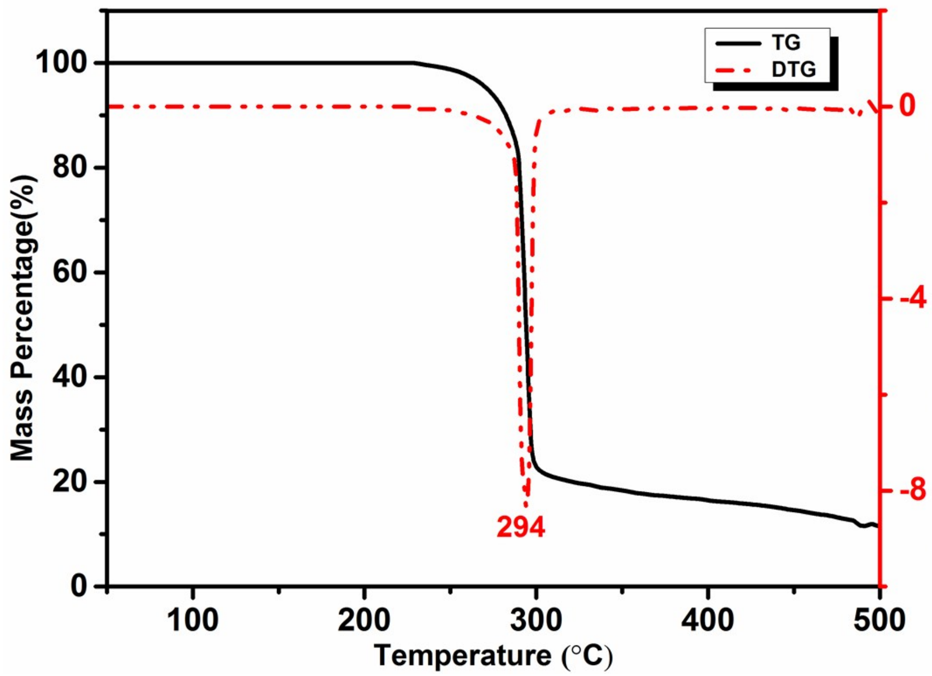

Fig. S17 TG-DTG curves (10 °C·min^{-1}) of **1**

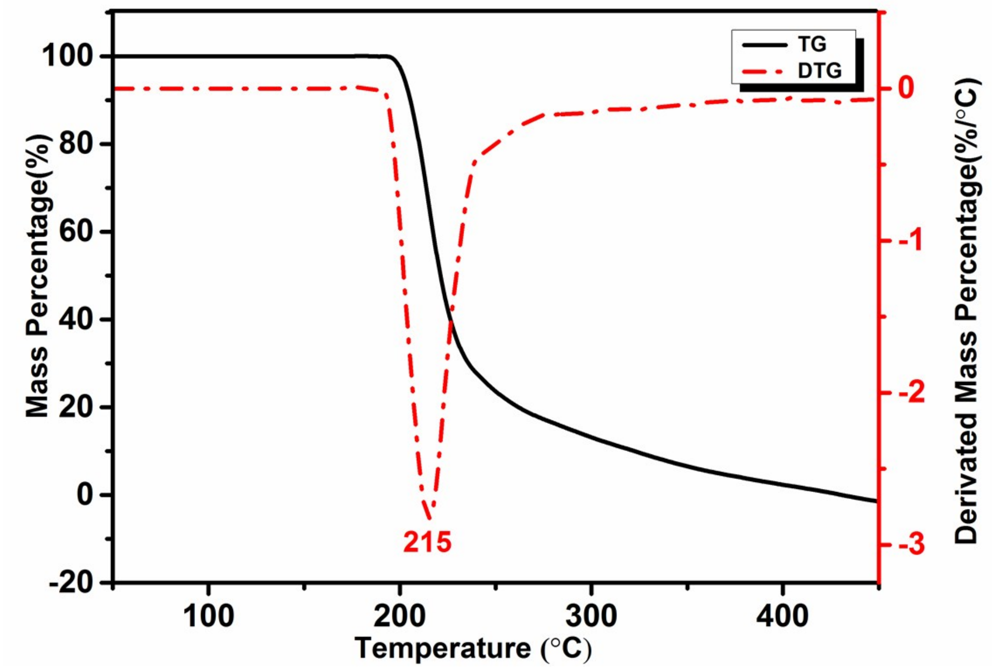

Fig. S18 TG-DTG curves (10 °C·min^{-1}) of **2**

8. Heats of formation

The calculations of the heats of formation were carried out using Gaussian 03 (Revision D.01) suite of programs. The geometric optimization and frequency analyses were calculated using B3LYP/6-31+G** level. The gas phase enthalpy of formation was obtained by using the atomization method based on G2 enthalpies. All of the optimized structures were characterized to be true local energy minima on the potential-energy surface without imaginary frequencies.

The solid-state enthalpy of formation was estimated by subtracting the heat of sublimation from gas-phase heat of formation. The heat of sublimation can be estimated with Trouton's rule according to equation 1[S7]:

$$\Delta H_{sub} = 188 / J \cdot mol^{-1} K^{-1} \times T \qquad \text{(equation 1)}$$

where T represents either the melting point or the decomposition temperature when no melting occurs prior to decomposition.

9. Non-isothermal kinetics analysis and thermodynamic analysis

The apparent activation energy and pre-exponential factor were calculated on the basis of the first exothermic decomposition peak temperature with three heating rates (5, 10, 15 $K \cdot min^{-1}$) by using Kissinger's method[S8] and Ozawa's method[S9]. The Kissinger's and Ozawa's equations are respectively established as follows.

$$\ln \beta / T_p = \ln AR / E_K + E_K / RT_p \qquad \text{(equation 2)}$$

$$\log \beta = \log AE_O / G(\alpha) R - 0.4567 \, E_O / RT_p - 2.315 \qquad \text{(equation 3)}$$

Where T_p is the peak temperature (K), R is the gas constant (8.314 $J \cdot K^{-1} \cdot mol^{-1}$), β is the linear heating rate ($K \cdot min^{-1}$), $G(\alpha)$ is the reaction mechanism function, A is the pre-exponential factor, E_K is the apparent activation energy in Kissinger's method, and E_O is the apparent activation energy in Ozawa's method.

The corresponding critical temperature of thermal explosion (T_b) according to Zhang's equations[S10], the values of the peak temperature while $\beta \to 0$ (T_{p0}), free energy of activation ($\Delta G^{\neq}$), the entropy of activation ($\Delta S^{\neq}$), and enthalpy of activation ($\Delta H^{\neq}$) were obtained. The equations for calculating are as follows, severally.

$$T_{pi} = T_{p0} + a\beta + b\beta^2 \qquad \text{(equation 4)}$$

$$T_b = (E_K - \sqrt{E_K^2 - 4E_K RT_{p0}}) / 2R \qquad \text{(equation 5)}$$

$$A = (k_B T_{p0} / h) \exp(1 + \Delta S^{\neq} / R) \qquad \text{(equation 6)}$$

$$\Delta H^{\neq} = E_K - RT_{p0} \qquad \text{(equation 7)}$$

$$\Delta G^{\neq} = \Delta H^{\neq} - T_{p0} \Delta S^{\neq} \qquad \text{(equation 8)}$$

Where a and b are coefficients, k_B is the Boltzmann constant (1.381×10^{-23} $J \cdot K^{-1}$) and h is the Planck constant (6.626×10^{-34} $J \cdot s$).

The peak temperatures and calculated results are listed in table S9. The Arrhenius equations can be expressed as $\ln k = 41.87 - 721.5 \times 10^3/(RT)$ for **1** and $\ln k = 31.63 - 235.8 \times 10^3/(RT)$ for **2**.

Table S9. Non-isothermal reaction kinetics and thermodynamic parameters of **1** and **2**

Non-isothermal reaction kinetics parameters			Thermodynamic parameters		
Kissinger's method				**1**	**2**
	1	**2**	T_{p0} (K)	553.85	472.75
E_K (kJ·mol^{-1})	721.5	235.8	T_b (K)	557.57	481.05
lg A_K	65.85	23.63	$\Delta S^{\neq}$ (J·K·mol^{-1})	98.08	14.19
R_K	-0.9928	-0.9999	$\Delta H^{\neq}$ (kJ·mol^{-1})	716.90	231.87
S_K	0.009273	0.008457	$\Delta G^{\neq}$ (kJ·mol^{-1})	662.57	225.16
Ozawa's method			Decomposition peak temperature		
	1	**2**		**1**	**2**
E_O (kJ·mol^{-1})	695.0	231.9	5 K·min^{-1}	285.3 °C	207.6 °C
R_O	-0.9930	-0.9999	10 K·min^{-1}	288.1 °C	213.2 °C
S_O	0.004028	0.003700	15 K·min^{-1}	289.1 °C	216.4 °C

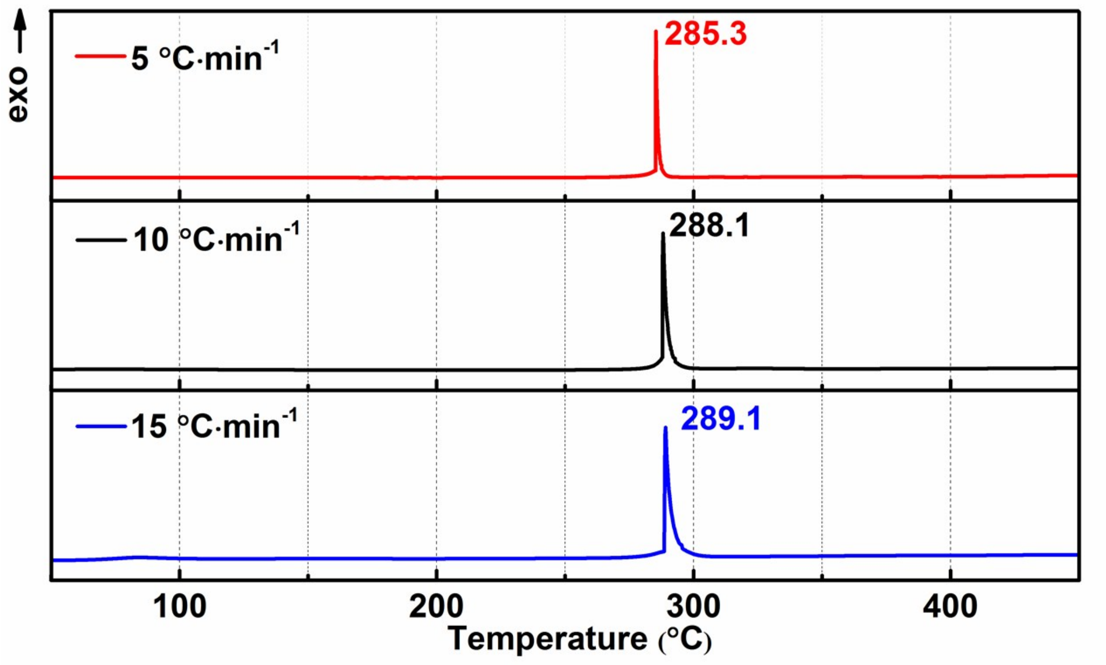

Fig. S19 DTA curves of **1**.

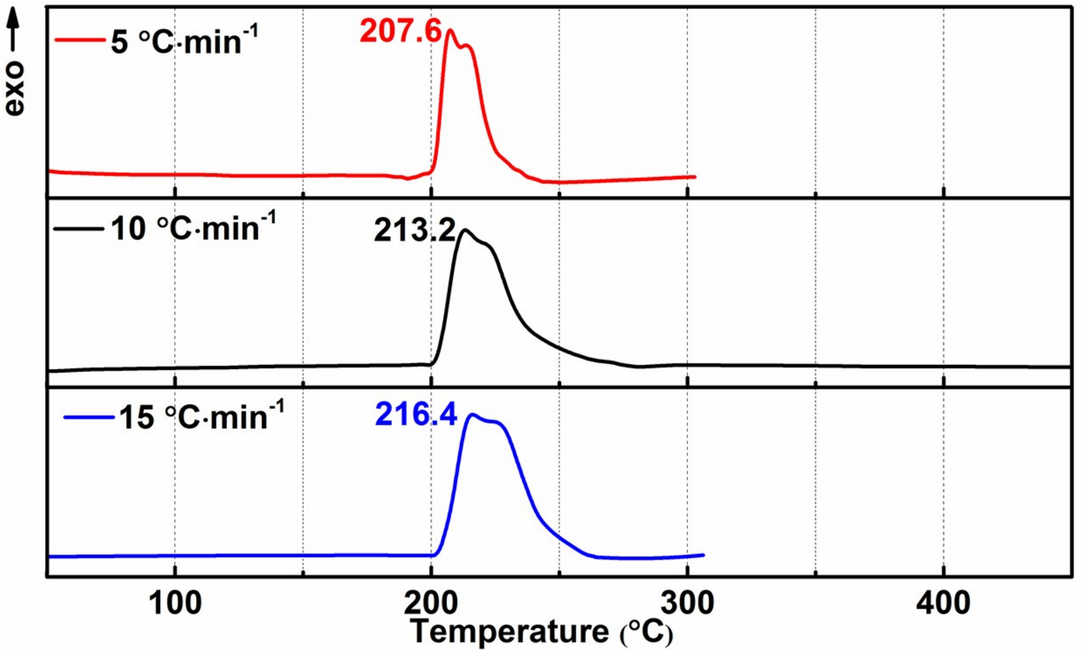

Fig. S20 DSC curves of **2**.

10. ICSS and LOL-π

To further explore more reasons for the combination of high thermal stability, high energy and low sensitivities of **1**, the nucleus independent chemical shift (NICS) and localized orbital locator-π (LOL-π) were calculated based on the optimized structures (using Gaussion 03 suite of programs) of **1** and TATB by employing the software Multiwfn v3.5. The visualized shielding maps, iso-chemical shielding surfaces (ICSS) and LOL-π diagrams were given in fig. S21. Obviously in fig. S21a and S21d, the shielding surfaces in **1** are larger and higher than that in TATB, indicating that **1** has a larger increased π conjugation than TATB. This could also be seen from their LOL-π diagrams (fig. S21b and S21e). Besides, the area of the high ICSS value at 20 ppm (pink) in **1** is even larger than that in TATB (fig. S21c and S21f), which supports the fact that **1** has high thermal stability and low sensitivities. The LOL-π diagrams (fig. S21c and S21f) shows that the π-electron orbits are incontinuous in **1**, which could explains the lower decomposition temperature of 1 than TATB.

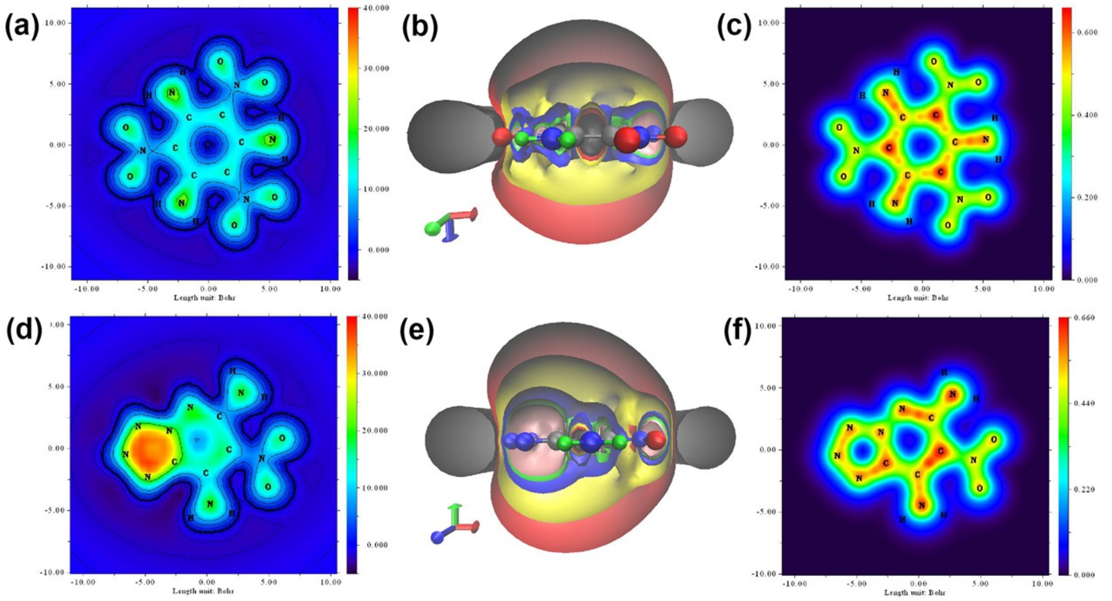

Fig. S21 (a) The shielding maps of TATB (1.89 bohr above the XY plane); (b) Clipping plane of TATB for multiple iso-chemcal shielding surfaces (ICSS, at 1 ppm in red; at 4 ppm in yellow; at 10 ppm in blue; at 16 ppm in green; at 20 ppm in pink; at -1 ppm in black); (c) LOL-π diagrams of TATB (1.2 bohr above the XY plane); (d) The shielding maps of **1** (1.89 bohr above the XY plane); (e) Clipping plane of **1** for multiple iso-chemcal shielding surfaces (ICSS, at 1 ppm in red; at 4 ppm in yellow; at 10 ppm in blue; at 16 ppm in green; at 20 ppm in pink; at -1 ppm in black); (f) LOL-π diagrams of **1** (1.2 bohr above the XY plane)

11. References

S1 M. J. Turner, J. J. McKinnon, S. K. Wolff, D. J. Grimwood, P. R. Spackman, D. Jayatilaka and M. A. Spackman, CrystalExplorer17 (2017). University of Western Australia. http://hirshfeldsurface.net

S2 T. Lu and F. Chen, *J. Comput. Chem.*, 2012, **33**, 580.

S3 W. Humphrey, A. Dalk and K. Schulten, *J. Molec. Graphics*, 1996, **14**, 33.

S4 O. V. Dolomanov, L. J. Bourhis, R. J. Gildea, J. A. K. Howard and H. Puschmann, *J. Appl. Cryst.*, 2009, **42**, 339.

S5 C. F. Macrae, P. R. Edgington, P. McCabe, E. Pidcock, G. P. Shields, R. Taylor, M. Towler and J. van de Streek, J. Appl. Cryst., 2006, 39, 453.

S6 Diamond - Crystal and Molecular Structure Visualization Crystal Impact - Dr. H. Putz & Dr. K. Brandenburg GbR, Kreuzherrenstr. 102, 53227 Bonn, Germany. http://www.crystalimpact.com/diamond

S7 M. S. Westwell, M. S.Searle, D. J.Wales, D. H.Wiliams, *J. Am. Chem. Soc.*, 1995, **117**, 5013.

S8 H. E. Kissinger, *Anal. Chem.*, 1957, **29**, 1702.

S9 T. Ozawa, *Chem. Soc. Jpn.*, 1965, **38**, 1881.

S10 T. Zhang, R. Hu, Y. Xie and F. Li, *Thermochim. Acta.*, 1994, **171**, 244.